

Heterogeneous & Homogeneous & Bio- & Nano-

# CHEM **CAT** CHEM

---

CATALYSIS

## Accepted Article

**Title:** Highly dispersed bimetallic nanoparticles supported on titanium carbides for remarkable hydrogen release from hydrous hydrazine

**Authors:** Tong Liu, Qingtao Wang, Jingzhi Yuan, Xue Zhao, and Guanhui Gao

This manuscript has been accepted after peer review and appears as an Accepted Article online prior to editing, proofing, and formal publication of the final Version of Record (VoR). This work is currently citable by using the Digital Object Identifier (DOI) given below. The VoR will be published online in Early View as soon as possible and may be different to this Accepted Article as a result of editing. Readers should obtain the VoR from the journal website shown below when it is published to ensure accuracy of information. The authors are responsible for the content of this Accepted Article.

**To be cited as:** *ChemCatChem* 10.1002/cctc.201701633

**Link to VoR:** <http://dx.doi.org/10.1002/cctc.201701633>

## COMMUNICATION

# Highly dispersed bimetallic nanoparticles supported on titanium carbides for remarkable hydrogen release from hydrous hydrazine

Tong Liu,<sup>[a],\*</sup> Qingtao Wang,<sup>[a]</sup> Jingzhi Yuan,<sup>[a]</sup> Xue Zhao,<sup>[a]</sup> and Guanhui Gao<sup>[b]</sup>

**Abstract:** Catalytic decomposition of hydrous hydrazine ( $N_2H_4 \cdot H_2O$ ) are considered as one of the promising candidate for fuel cell field, but the sluggish reaction kinetics dramatically impede their practical application. In this study, bimetallic RhNi nanoparticles are successfully anchored on titanium carbides (MXene) by one-step wet-chemical method, building a block for superior catalysts toward hydrous hydrazine ( $N_2H_4 \cdot H_2O$ ) decomposition applying for chemical hydrogen storage. The synthesized RhNi/MXene catalysts are characterized by XPS, TEM, STEM-HAADF and ICP-AES. Due to the particles size and synergistic effect, the  $Rh_{0.8}Ni_{0.2}/MXene$  nanocatalysts demonstrate 100%  $H_2$  selectivity, excellent durability, and high reaction kinetics with turnover frequency value of  $857 h^{-1}$  toward  $N_2H_4 \cdot H_2O$  decomposition in alkaline solution.

Very recently, the worldwide concerns on energy crisis and environmental pollution have stimulated intensive attention, which is essential to pursue sustainable and renewable energy.<sup>[1-7]</sup> Catalytic hydrogen generation from hydrogen storage materials is regarded as a promising way to address the energy and environmental crisis, due to its advantages of light weight, high abundance and chemical energy per mass.<sup>[8-14]</sup> Among numerous hydrogen storage materials, hydrous hydrazine ( $N_2H_4 \cdot H_2O$ ) has attracted much attention due to its high hydrogen density of 8.0 wt%, low molecular weight of 50.1 g/mol and excellent stability under ambient conditions.<sup>[15-21]</sup> Therefore, it is considered as one of the most leading candidate in promising chemical hydrogen-storage materials. The two molar CO-free  $H_2$  is able to efficiently release from one molar hydrous hydrazine according to the following reaction  $H_2NNH_2 \rightarrow N_2 + 2H_2$  (Eqn (1)), while the undesired reaction pathway ( $3H_2NNH_2 \rightarrow N_2 + 4NH_3$ , eqn 2) must be avoided, because the generated  $NH_3$  is poisonous to the fuel-cell catalysts.<sup>[22-25]</sup> In order to achieve the high efficiency of dehydrogenation from hydrous hydrazine, it is essential to develop catalysts with high selectivity only the catalytic hydrogenation (Eqn (1)) occurring. Although much effort has been engaged to improve the reaction rate and obtain high efficiency with 100 %  $H_2$  selectivity, the kinetics of catalytic  $N_2H_4 \cdot H_2O$  decomposition is not acceptable.

Recently, graphene-like transition metal carbide (MXene,  $Ti_3C_2(OH)_x(F_{1-x})_2$ ) has been widely investigated as a promising support for new nano-catalysts. The abundant functional groups

on MXene surface, such as Ti-OH and Ti-F bonds, not only stabilize the nanoparticles during reduction, but also improve the hydrophilicity of the resultant catalysts.<sup>[26-31]</sup> However, there were a few literatures reported on MXene anchoring nanocatalysts only the typical study on MXene supported Ru-based nanocatalysts were prepared and applied as excellent nanocatalysts for sodium borohydride and ammonia borane decompositions.<sup>[32,33]</sup> Here, we creatively synthesize the RhNi bimetallic nanoparticles supported on MXene via one-step wet-chemical approach. Unexpectedly, the resultant RhNi/MXene nano-catalysts with 100% of  $H_2$  selectivity indicate an extremely high catalytic activity and excellent durability toward decomposition of  $N_2H_4 \cdot H_2O$ .

Figure. S1 shows the preparation of the RhNi/MXene nanocatalyst. In a typical experiment, 100 mg MXene is dissolved in 2 mL water in a two-neck round-bottom flask (30 mL), with sonicating for 30 min to obtain a uniform dispersion. Then, 100  $\mu$ L rhodium chloride solution (0.8 mmol/mL) and 100  $\mu$ L nickel chloride (0.2 mmol/mL) are both added into above MXene solution gently, with electromagnetic stirring (speed of 220 rpm) for 20 min. Then, 24 mg of sodium borohydride ( $NaBH_4$ ) ( $1.3 mol L^{-1}$ ) dissolved in 0.5 mL of 2.0 M NaOH solution is quickly added into above resulted mixture under vigorous stirring for 3 h at 0 °C using an ice bath to maintain the temperature for prevention of RhNi NPs aggregation. The RhNi/MXene nanocatalysts are obtained by washing with deionized water and centrifugation. The corresponding macroscopic photos are shown in Figure S2.

The powder X-ray diffraction (PXRD) patterns of the as-synthesized RhNi/MXene are measured (Figure. S3). The pattern peaks at 29.8°, 35.3°, and 36.9° are assigned to MXene. In addition, the peaks of RhNi are very small and broad, indicating that the ultrafine RhNi NPs are successfully supported on MXene. Additionally, for the six samples with different compositions, it can be found that the corresponding XRD diffraction peaks gradually shift to higher  $2\theta$  as the Ni composition increases. These results clearly demonstrate that our obtained particles are RhNi alloys. Figure. S4 exhibits the measured XPS spectra of RhNi/MXene in the Rh 3d, Ni 2p, Ti 2p, O 1s, F 1s and C 1s regions, respectively. The peaks at 284.5 eV and 281.6 eV are attributed to the binding energy of C 1s. Additionally, the peaks corresponding to F and O indicate the introduction of functional groups such as OH and F. The two peaks located at 307.3 eV and 311.8 eV could be assigned to elemental  $Rh^0 3d_{5/2}$  and  $Rh^0 3d_{3/2}$ , respectively. While the Ni peaks corresponding to  $Ni^0 2p_{1/2}$  and  $Ni^0 2p_{3/2}$  are observed at 851.9 and 870.3 eV.<sup>[32,33]</sup> These results clearly demonstrate that the RhNi particles have been successfully anchored on MXene surface. Additionally, compared to Rh/MXene, the binding energies of Rh 3d in RhNi/MXene are negatively shifted (Figure. S5a). In contrast, the binding energies of Ni 2p in RhNi/MXene are positively shifted relative to that of Ni/MXene (Figure. S5b). These shifts of the binding energies indicate the formation of RhNi alloy and electron transferring from Ni to Rh, which benefits to

[a] Dr. T. Liu, Q.-T. Wang, J.-Z. Yuan, X. Zhao  
College of Materials Science and Engineering  
Qingdao University of Science and Technology  
53 Zhengzhou Rd, Qingdao, 266000, PR China  
E-mail: liutong@qust.edu.cn

[b] Dr. G.-H. Gao  
Paul-Drude-Institut für Festkörperelektronik  
Hausvogteiplatz 5–7, 10117 Berlin, Germany

## COMMUNICATION

enhancing the synergistic effect in metallic catalyst, resulting in improvement for catalytic property.

Furthermore, the d-spacing of RhNi NPs is approximately 0.212 nm, which is between 0.219 nm of Rh (111) and 0.203 nm of Ni (011) (Figure. 1c), indicating that the obtained nanoparticles are RhNi alloys. In addition, the metal loading for the Rh<sub>0.8</sub>Ni<sub>0.2</sub>/MXene is determined by inductively coupled plasma-atomic emission spectroscopy (ICP-AES) to be 9.8 wt%, and the the relative compositions of the RhNi NPs yield the following compositions: 82 at% Rh, and 17 at% Ni, in the Rh<sub>0.8</sub>Ni<sub>0.2</sub>/MXene. Figure. S6 demonstrates the N<sub>2</sub> adsorption-desorption isotherms of Rh<sub>0.8</sub>Ni<sub>0.2</sub>/MXene. The measured Brunauer-Emmett-Teller (BET) surface area of the RhNi/MXene is calculated to 77.83 m<sup>2</sup> g<sup>-1</sup> due to graphene oxide partially avoided. Moreover, the Barrett-Joyner-Halenda (BJH) analysis shows that the average pore diameter is 3.6 nm with the pore volume of 0.016 cm<sup>3</sup> g<sup>-1</sup>.

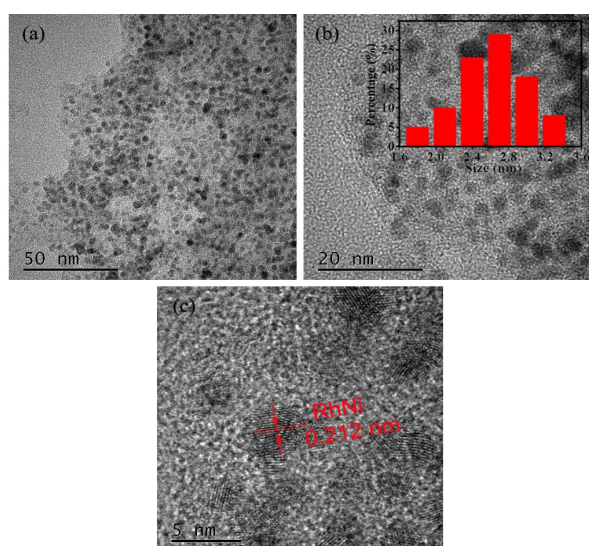


**Figure 1.** TEM (a, b) and HRTEM images of the Rh<sub>0.8</sub>Ni<sub>0.2</sub>/MXene (c).

TEM and high resolution TEM (HRTEM) are carried out to further investigate the morphologies of RhNi NPs. The TEM and HRTEM (Figure. 1) images of RhNi/MXene indicate that the discrete RhNi NPs homogeneously disperse on MXene surface with an average size of 2.8 nm (Figure. 1b inside). The elemental mappings of Ni, Rh, C, O and Ti (Figure. 2) reveal that metal and non-metal elements uniformly disperse throughout the whole MXene. The formation of mono-dispersed RhNi NPs benefits to enhancing catalytic property for N<sub>2</sub>H<sub>4</sub>·H<sub>2</sub>O decomposition.

The catalytic performances of Rh<sub>x</sub>Ni<sub>1-x</sub>/MXene (0 ≤ x ≤ 1) for H<sub>2</sub> generation from N<sub>2</sub>H<sub>4</sub>·H<sub>2</sub>O are investigated at 50 °C with a constant molar ratio of catalyst/N<sub>2</sub>H<sub>4</sub>·H<sub>2</sub>O = 0.067 (Figure. 3). It can be seen that the catalytic activity and H<sub>2</sub> selectivity are strongly dependent on the metallic Rh/Ni molar ratio. Neither Ni nor Rh shows high catalytic property, however, by alloying small amount of Ni to Rh, both of H<sub>2</sub> selectivity and kinetics rate of the catalysts obviously is dramatically enhanced. Reasonably, the remarkable catalytic activity is attributed to the molecular-scale synergistic effect in RhNi alloy, which could enhance the electronic effects of nanocatalysts. For all the bimetallic Rh<sub>x</sub>Ni<sub>1-x</sub>/MXene (0 ≤ x ≤ 1) catalysts investigated, the Rh<sub>0.8</sub>Ni<sub>0.2</sub>/MXene exhibits excellent catalytic activity, the corresponding TOF value can

achieve 857 h<sup>-1</sup> at 50 °C, which is rather higher than those of reported values in Table 1.

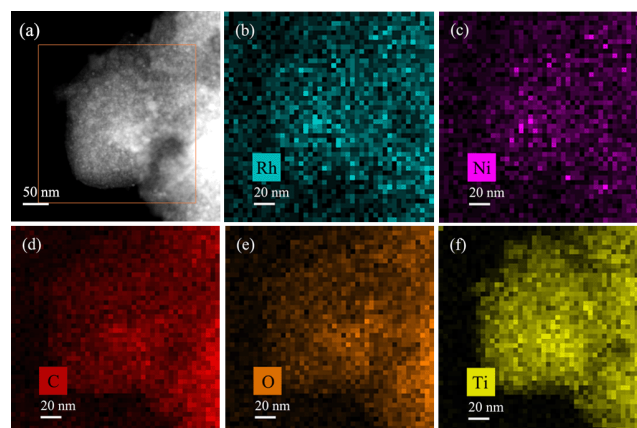


**Figure 2.** The STEM-HAADF images of the Rh<sub>0.8</sub>Ni<sub>0.2</sub>/MXene (a) and the corresponding elemental mapping images for Rh (b), Ni (c), C (d), O (e) and Ti (f).

**Table 1.** T Catalytic activities of different catalysts for the dehydrogenation of hydrous hydrazine

Catalyst	Solvent/medium	Temp. (°C)	Selectivity H <sub>2</sub> for (100 %)	TOF (h <sup>-1</sup> )	Ea (kJ mol <sup>-1</sup> )	Ref.
Rh <sub>0.8</sub> Ni <sub>0.2</sub> /MXene	Aqueous NaOH	50	100	857	38.2	This work
Rh <sub>55</sub> Ni <sub>45</sub> /Ce(OH)	Aqueous NaOH	50	100	395	38.8	34
Rh <sub>14</sub> Ni/graphene	Aqueous NaOH	30	100	28		18
Rh <sub>34</sub> Ni <sub>66</sub> @ZIF-8	Aqueous NaOH	50	100	140	58.1	35
Pt <sub>0.6</sub> Ni <sub>0.4</sub> /PDA-rGO	Aqueous NaOH	50	100	2056	33.39	36
(Ni <sub>1</sub> Pt <sub>7</sub> ) <sub>0.5</sub> -(MnO <sub>x</sub> ) <sub>0.5</sub> /NPC-900	Aqueous NaOH	50	100	706	50.15	37
Ni <sub>88</sub> Pt <sub>12</sub> /MIL-101	Aqueous NaOH	50	100	471	40.4	38
Ni <sub>0.8</sub> Pt <sub>0.2</sub> /MIL-101-NH <sub>2</sub>	Aqueous NaOH	50	100	676	53.2	11
Ni <sub>3</sub> Pt <sub>7</sub> /BNG-1000	Aqueous NaOH	30	100	199.4	28.4	39
Ni <sub>0.9</sub> Pt <sub>0.05</sub> Rh <sub>0.05</sub> /La <sub>2</sub> O <sub>3</sub>	Aqueous NaOH	25	100	45.9		40
Ni <sub>0.9</sub> Pt <sub>0.1</sub> /Ce <sub>2</sub> O <sub>3</sub>	Aqueous NaOH	25	100	28.1	42.3	19
Ni <sub>6</sub> Pt <sub>4</sub> -SF	Aqueous NaOH	25	100	150		41
Pt <sub>60</sub> Ni <sub>40</sub> -CNDs	Aqueous NaOH	50	100	170	43.9	42
Ni <sub>0.55</sub> Pt <sub>0.45</sub> /graphene	Aqueous NaOH	30	100	434	23.9	43
Ni <sub>0.9</sub> Pt <sub>0.1</sub> /MIL-101	Aqueous NaOH	30	100	140	48.4	44
Rh <sub>0.8</sub> Ni <sub>0.2</sub> @CeO <sub>x</sub> /rGO	Aqueous NaOH	30	100	36.4	58	45

Mass spectrometry (MS) results further confirm the formation of H<sub>2</sub> and N<sub>2</sub> and the absence of NH<sub>3</sub> in the released gas (Figure. S7). Remarkably, the high catalytic activity is attributed to the formation of small monodispersed RhNi NPs. As shown in Figure. 1b-c, small RhNi NPs with size of 2.8 nm uniformly dispersed on MXene surface without aggregation is observed, which could provide more active sites for reaction, efficiently improving performance for N<sub>2</sub>H<sub>4</sub>·H<sub>2</sub>O decomposition. Additionally, the synergistic effect between Rh and Ni could promote the catalytic activity. The synergistic effect between bimetallic nanoparticles can efficiently tune surface electronic states of bimetallic nanoparticles, particularly related to local strain and effective atomic coordination number at the surface, leading an apparent improvement for N<sub>2</sub>H<sub>4</sub>·H<sub>2</sub>O decomposition.<sup>[46]</sup>

## COMMUNICATION

Furthermore, the support material plays an important role on determining the catalytic performance for  $N_2H_4 \cdot H_2O$  decomposition.<sup>[47,48]</sup> In order to evaluate the effect of the supported materials on the catalytic performances toward the  $N_2H_4 \cdot H_2O$  decomposition, catalysts are synthesized by loading RhNi NPs on different carriers such as GO ( $Rh_{0.8}Ni_{0.2}/GO$ ), XC-72 ( $Rh_{0.8}Ni_{0.2}/XC-72$ ), MCNTs ( $Rh_{0.8}Ni_{0.2}/MCNTs$ ),  $Al_2O_3$  ( $Rh_{0.8}Ni_{0.2}/Al_2O_3$ ), and support-free ( $Rh_{0.8}Ni_{0.2}$ ). As shown in Figure. S8, their catalytic performance toward  $N_2H_4 \cdot H_2O$  decomposition are inferior to that of  $Rh_{0.8}Ni_{0.2}/MXene$ , which is attributed to the strong synergistic effect between nanocatalyst and MXene support. To demonstrate the effect of MXene support on improving catalytic activity, we measured the binding energies of Rh 3d and Ni 2p in RhNi/MXene and support free RhNi. As shown in Figure. S9, the binding energies of Rh 3d and Ni 2p in RhNi/MXene are both negatively shifted compared to those of support free RhNi, suggesting that MXene promote electron transfer to RhNi, and benefit the cleavage of N-H bonds.<sup>[22,42]</sup> These above results clearly illustrate that MXene, as a superior support, would improve cooperative effect toward RhNi NPs and facilitates dehydrogenation of aqueous solution of  $N_2H_4 \cdot H_2O$  in our system.

In order to obtain the activation energy ( $E_a$ ) of the  $N_2H_4 \cdot H_2O$  decomposition catalysed by  $Rh_{0.8}Ni_{0.2}/MXene$  catalysts, the reactions at different temperatures (25–60 °C) are carried out and the corresponding results are shown in Figure. S10a. From the results, the hydrogen generation rate over the  $Rh_{0.8}Ni_{0.2}/MXene$  catalyst greatly depends on the reaction temperatures, which is agreed to the previous works.<sup>[49–52]</sup> The catalytic reactions at 25, 35, 40, 50, and 60 °C demonstrate the corresponding TOF values of 245, 443, 507, 857, and 1204  $h^{-1}$ . The Arrhenius plot of  $\ln$  TOF vs.  $1/T$  for this catalyst is plotted in Figure. S10b, which  $E_a$  is calculated as 38.2  $kJ \cdot mol^{-1}$ .

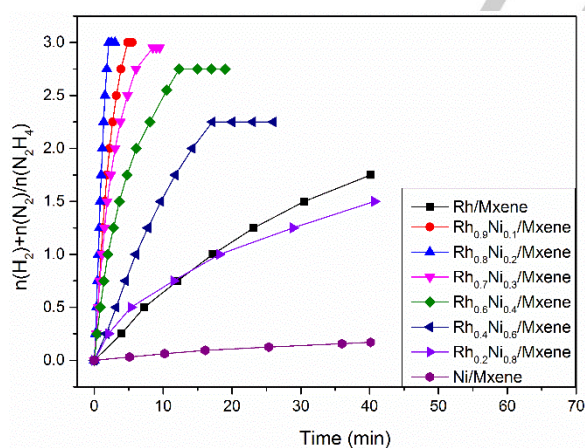


**Figure 3.** Time course plots for  $H_2$  generation from  $N_2H_4 \cdot H_2O$  decomposition with different Rh/Ni molar ratios ( $0 \leq x \leq 1$ ) at 50 °C. The molar ratio of metal/ $N_2H_4 \cdot H_2O = 0.067$ .

It is found that the  $N_2H_4 \cdot H_2O$  decomposition can be promoted by controlling the concentration of NaOH in reaction system. The hydrogen generation from  $N_2H_4 \cdot H_2O$  with/without adding NaOH is investigated comparatively. As shown in Figure. S11, the reaction kinetics is sluggish without NaOH. After addition of NaOH, the reaction rate obviously increases, reaching a maximum TOF value of 857  $h^{-1}$  and 100 % at the NaOH concentration of 2 M. The

possible reason for the effects of the NaOH additive may be explained as below: the addition of NaOH will decrease the undesired  $N_2H_5^+$  concentration in the aqueous solution. Additionally, in view of the chemical equilibrium, a strong alkaline environment will inhibit the generation of the basic byproduct  $NH_3$ , which raises the  $H_2$  selectivity.<sup>[53–56]</sup>

For the practical application of catalysts, the durability/stability of catalysts is the key point. Therefore, the durability of the  $Rh_{0.8}Ni_{0.2}/MXene$  nanocatalyst up to sixth run for  $N_2H_4 \cdot H_2O$  decomposition is characterized by adding additional aliquots (1.5 mmol) of  $N_2H_4 \cdot H_2O$  to the catalyst after the reaction completion for the last run. It is evident from Figure. 4a, we can find that the catalytic activity of the as-prepared  $Rh_{0.8}Ni_{0.2}/MXene$  nanocatalyst has no obvious decrease after a six-time recycle test, indicating the as-prepared  $Rh_{0.8}Ni_{0.2}/MXene$  possesses a high durability in  $N_2H_4 \cdot H_2O$  decomposition. Furthermore, the in situ synthesized NPs are magnetic and thus can be separated from the reaction solution by an external magnet (Figure. 4b), which prove the practical recycling application of the NPs more convenient. The stable durability of  $N_2H_4 \cdot H_2O$  is mainly attributed to dispersive metallic RhNi NPs without any aggregation of, which is proved by TEM measurement. As clearly seen from the TEM images (Figure. 4c-d), there is no obvious aggregation of the RhNi NPs on MXene, further confirming the advantage of the confinement effect of MXene.

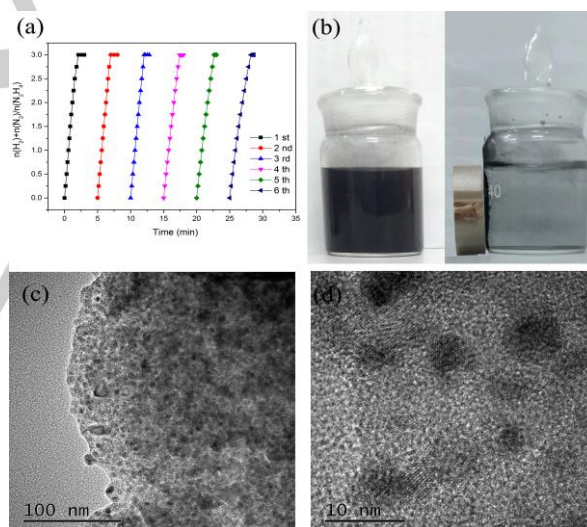


**Figure 4.** Time course plots for  $H_2$  generation from  $N_2H_4 \cdot H_2O$  decomposition catalyzed by  $Rh_{0.8}Ni_{0.2}/MXene$  from 1st to 6th cycles (a); photographs of the  $Rh_{0.8}Ni_{0.2}/MXene$  before (left) and after (right) the magnetic separation (b); and TEM image of the  $Rh_{0.8}Ni_{0.2}/MXene$  NPs after the sixth cycle (c, d).

In summary, monodispersed RhNi NPs are successfully anchored on MXene surfaces via a facile one-step wet-chemical strategy. By optimizing the fraction of Rh component in Rh-Ni system, the synthesized  $Rh_{0.8}Ni_{0.2}/MXene$  catalysts demonstrate the most reactive function to  $N_2H_4 \cdot H_2O$  decomposition with 100 % of  $H_2$  selectivity and excellent catalytic performance of 857  $h^{-1}$  at 50 °C. Additionally, the synthesized  $Rh_{0.8}Ni_{0.2}/MXene$  shows superior catalytic performance to that of  $Rh_{0.8}Ni_{0.2}/GO$ ,  $Rh_{0.8}Ni_{0.2}/XC-72$ ,  $Rh_{0.8}Ni_{0.2}/MCNTs$ ,  $Rh_{0.8}Ni_{0.2}/Al_2O_3$ , and  $Rh_{0.8}Ni_{0.2}$ . Kinetic studies on  $N_2H_4 \cdot H_2O$  decomposition catalyzed over  $Rh_{0.8}Ni_{0.2}/MXene$  demonstrate that the factors of metallic

## COMMUNICATION

particle size, catalyst amount, support effect and NaOH concentration have positive effects on the reaction rate. Moreover, the obtained nanocatalysts possess a stable durability of  $\text{N}_2\text{H}_4 \cdot \text{H}_2\text{O}$  decomposition. This simple synthetic approach can be easily extended to facile preparation for other MXene supported metal NPs.

## Acknowledgements

This work was financially supported by the National Natural Science Foundation of China (Project Nos. 51306166 and 51206101).

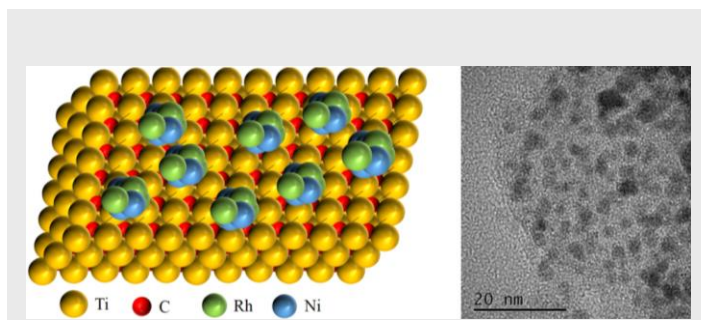
**Keywords:** heterogeneous catalysis • dehydrogenation • RhNi nanoparticles • titanium carbides • Synergistic effect

- 1 S. Young, *Nature* **2001**, *414*, 487-488.
- 2 P. P. Edwards, L. Kuznetsov, N. P. Brandon, *Energy Policy* **2008**, *36*, 4356-4362.
- 3 X. Yang, Q. Xu, *Chinese J. Catal.*, **2016**, *37*, 1594-9159.
- 4 H. L. Wang, Q. L. Zhu, R. Zou, Q. Xu, *Chem*, **2017**, *2*, 52-80.
- 5 J. Kotowicz, L. Bartela, D. Wecel, K. Dubiel, *Energy* **2017**, *118*, 156-171.
- 6 L. Yang, W. Luo, G. Cheng, *ACS Appl. Mater. Interfaces* **2013**, *5*, 8231-8240.
- 7 W. Li, X. Wang, D. Xiong, L. Liu, *Int. J. Hydrogen Energy* **2016**, *41*, 9344-9354.
- 8 H. Dai, Y. Qiu, H. Dai, P. Wang, *Int. J. Hydrogen Energy*, **2017**, *42*, 16355-16361.
- 9 J. Cheng, X. Gu, P. Liu, H. Zhang, L. Ma, H. Su, *Appl. Catal. B-Environ.* **2017**, *218*, 460-469.
- 10 J. Liang, L. J. Gao, N. N. Miao, Y. J. Chai, N. Wang, X. Q. Song, *Energy* **2017**, *113*, 282-287.
- 11 P. L. Liu, X. J. Gu, Y. Y. Wu, J. Cheng, H. Q. Su, *Int. J. Hydrogen Energy* DOI: <http://dx.doi.org/10.1016/j.ijhydene.2017.06.191>
- 12 H. M. Chen, C. K. Chen, R. S. Liu, L. Zhang, J. Zhang, D. P. Wilkinson, *Chem. Soc. Rev.* **2012**, *41*, 5654-5671.
- 13 J. Graetz, *Chem. Soc. Rev.* **2009**, *38*, 73-82.
- 14 G. Nong, M. Li, Y. Y. Chen, Z. W. Zhou, S. F. Wang, *Energy* **2016**, *81*, 4712-4716.
- 15 S. K. Singh, X. B. Zhang, Q. Xu, *J. Am. Chem. Soc.* **2009**, *131*, 9894-9595.
- 16 A. K. Singh, Q. Xu, *Int. J. Hydrogen Energy* **2014**, *39*, 9128-9134.
- 17 S. K. Singh, Q. Xu, *J. Am. Chem. Soc.* **2009**, *131*, 18032-18033.
- 18 J. Wang, X. B. Zhang, Z. L. Wang, L. M. Wang, Y. Zhang, *Energy Environ. Sci.* **2012**, *5*, 6885-6888.
- 19 H. L. Wang, J. M. Yan, Z. L. Wang, O. Song-Il, Q. Jiang, *J. Mater. Chem. A* **2013**, *1*, 14957-14962.
- 20 L. He, Y. Huang, A. Wang, X. Wang, X. Chen, J. J. Delgado, T. Zhang, *Angew. Chem. Int. Ed.* **2012**, *51*, 6191-6198.
- 21 L. He, B. L. Liang, L. Li, X. F. Yang, Y. Q. Huang, A. Q. Wang, X. D. Wang, T. Zhang, *ACS Catal.* **2015**, *5*, 1623-1628.
- 22 Q. L. Zhu, Q. Xu, *Energy Environ. Sci.* **2015**, *8*, 478-512.
- 23 H. B. Dai, Y. J. Zhong, P. Wang, *Prog. Nat. Sci. Mater.* **2017**, *27*, 121-125.
- 24 K. V. Manukyan, A. Cross, S. Rouvimov, J. Millerc, A. S. Mukasyan, E. E. Wolf, *Appl. Catal. A* **2014**, *476*, 47-53.
- 25 P. P. Zhao, N. Cao, J. Su, W. Luo, G. Z. Cheng, *ACS Sustain Chem. Eng.* **2015**, *3*, 1086-1093.
- 26 X. Xie, S. Chen, W. Ding, Y. Nie, Z. Wei, *Chem. Commun.* **2013**, *49*, 10112-10114.
- 27 M. Naguib, J. Come, B. Dyatkin, V. Presser, P.-L. Taberna, P. Simon, *Electrochem. Commun.* **2012**, *16*, 61-64.
- 28 X. Xie, Y. Xue, L. Li, S. Chen, Y. Nie, W. Ding, Z. D. Wei, *Nanoscale* **2014**, *6*, 11035-11040.
- 29 M. Ghidui, M. R. Lukatskaya, M. Q. Zhao, Y. Gogotsi, M. W. Barsoum, *Nature* **2014**, *516*, 78-81.
- 30 M. Naguib, M. Kurtoglu, V. Presser, J. Lu, J. Niu, M. Heon, L. Hultman, Y. Gogotsi, M. W. Barsoum, *Adv. Mater.* **2011**, *23*, 4248-4253.
- 31 Q. Peng, J. Guo, Q. Zhang, J. Xiang, B. Liu, A. Zhou, R. Liu, Y. Tian, *J. Am. Chem. Soc.* **2014**, *136*, 4113-4116.
- 32 X. Li, G. Fan, C. Zeng, *Int. J. Hydrogen Energy* **2014**, *39*, 14927-17934.
- 33 X. Li, C. Zeng, G. Fan, *Int. J. Hydrogen Energy* **2015**, *40*, 3883-3891.
- 34 J. Chen, Q. Yao, J. Zhu, X. Chen, Z. H. Lu, *Int. J. Hydrogen Energy* **2016**, *41*, 3946-3954.
- 35 B. Q. Xia, N. Cao, H. M. Dai, J. Su, X. J. Wu, W. Luo, G. Z. Cheng, *ChemCatChem* **2014**, *6*, 2549-2552.
- 36 F. Z. Song, Q. L. Zhu, Q. Xu, *J. Mater. Chem. A* **2015**, *3*, 23090-23094.
- 37 Y. J. Ma, H. Wang, H. Li, J. L. Key, S. Ji, R. F. Wang, *RSC Adv.* **2014**, *4*, 20722-20728.
- 38 X. Du, S. Tan, P. Cai, W. Luo, G. Cheng, *J. Mater. Chem. A* **2016**, *4*, 14572-14576.
- 39 X. Du, C. Du, P. Cai, W. Luo, G. Cheng, *ChemCatChem* **2016**, *8*, 1410-1416.
- 40 O. Song-Il, J. M. Yan, H. L. Wang, Z. L. Wang, Q. Jiang, *Int. J. Hydrogen Energy* **2014**, *39*, 3755-3761.
- 41 B. Xia, T. Liu, W. Luo, G. Cheng, *J. Mater. Chem. A* **2016**, *4*, 5616-5622.
- 42 J. K. Sun, Q. Xu, *ChemCatChem* **2015**, *7*, 526-531.
- 43 J. M. Chen, Z.-H. Lu, W. Huang, Z. B. Kang, X. S. Chen, *J. Alloy. Compd.* **2017**, *695*, 3036-3043.
- 44 Z. J. Zhang, S. L. Zhang, Q. L. Yao, X. S. Chen, Z.-H. Lu, *Inorg. Chem.* **2017**, *56*, 11938-11945.
- 45 Z. J. Zhang, Z.-H. Lu, H. L. Tan, X. S. Chen, Q. L. Yao, *J. Mater. Chem. A* **2015**, *3*, 23520-23529.
- 46 H. L. Jiang, Q. Xu, *J. Mater. Chem.* **2011**, *21*, 13705-13725.
- 47 M. S. Kim, S. H. Chung, C. J. Yoo, M. S. Lee, I. H. Cho, D. W. Lee, K. Y. Lee, *Appl. Catal. B Environ.* **2013**, *142*, 354-361.
- 48 P. Luksirikul, K. Tedsree, M. G. Moloney, M. L. H. Green, S. C. H. Tsang, *Angew. Chem. Int. Ed.* **2012**, *51*, 6998-7001.
- 49 O. Song-Il, J. M. Yan, H. L. Wang, Z. L. Wang, Q. Jiang, *J. Power Sources* **2014**, *262*, 386-390.
- 50 D. G. Tong, D. M. Tang, W. Chu, G. F. Gu, P. Wu, *J. Mater. Chem. A* **2013**, *1*, 6425-6432.
- 51 L. He, B. Liang, L. Li, X. Yang, Y. Huang, A. Wang, *ACS Catal.* **2015**, *5*, 1623-1628.
- 52 D. C. Zhong, Y. L. Mao, X. Tan, P. Zhong, L. X. Liu, *Int. J. Hydrogen Energy* **2016**, *41*, 6362-6368.
- 53 X. Miao, M. M. Chen, W. Chu, P. Wu, D. G. Tong, *ACS Appl. Mater. Interfaces* **2016**, *8*, 25268-25278.
- 54 H. Dai, H. B. Dai, Y. J. Zhong, Q. Kang, L. X. Sun, P. Wang, *Int. J. Hydrogen Energy* **2017**, *42*, 5684-5693.
- 55 L. He, Y. Huang, A. Wang, Y. Liu, X. Liu, X. Chen, J. J. Delgado, X. D. Wang, T. Zhang, *J. Catal.* **2013**, *298*, 1-9.
- 56 C. C. Liu, J. M. Song, J. F. Zhao, H. J. Li, H. S. Qian, H. L. Niu, C. J. Mao, S. Y. Zhang, Y. H. Shen, *Appl. Catal. B Environ.* **2012**, *119-120*, 139-45.

## COMMUNICATION

Entry for the Table of Contents (Please choose one layout)

## COMMUNICATION



Tong Liu,\*, Qingtao Wang, Jingzhi Yuan, Xue Zhao, and Guanhui Gao,\*

Page 1. – Page 5.

**Highly dispersed bimetallic nanoparticles supported on titanium carbides for remarkable hydrogen release from hydrous hydrazine**

Bimetallic RhNi nanoparticles are successfully anchored on titanium carbides (MXene), building a block for superior catalysts toward hydrous hydrazine decomposition applying for chemical hydrogen storage. Due to the particles size and synergistic effect, the  $\text{Rh}_{0.8}\text{Ni}_{0.2}/\text{MXene}$  nanocatalysts demonstrate high selectivity, excellent durability, and high reaction kinetics with turnover frequency value of  $857 \text{ h}^{-1}$  in alkaline solution.